

Article

Experimental Research on the Mechanical Properties of Methane Hydrate-Ice Mixtures

Yanghui Li, Yongchen Song *, Weiguo Liu and Feng Yu

Key Laboratory of Ocean Energy Utilization and Energy Conservation of Ministry of Education, Dalian University of Technology, Dalian 116024, China; E-Mails: li.yanghui@mail.dlut.edu.cn (Y.L.); liuwg@dlut.edu.cn (W.L.); fengyu@mail.dlut.edu.cn (F.Y.)

* Author to whom correspondence should be addressed; E-Mail: songyc@dlut.edu.cn; Tel./Fax: +86-411-84708015.

Received: 8 December 2011; in revised form: 11 January 2012 / Accepted: 17 January 2012 / Published: 30 January 2012

Abstract: The mechanical properties of methane hydrate are important to the stability of borehole and methane extraction from a methane hydrate reservoir. In this study, a series of triaxial compression tests were carried out on laboratory-formed methane hydrate-ice mixtures with various methane hydrate contents. Axial loading was conducted at an axial strain rate of 1.33%/min and a constant temperature of $-10\text{ }^{\circ}\text{C}$. The results indicate that: (1) the deformation behavior is strongly affected by confining pressure and methane hydrate content; (2) the failure strength significantly increases with confining pressure when confining pressure is less than 10 MPa, and decreases with methane hydrate content; (3) the cohesion decreases with methane hydrate content, while the internal friction angle increases with methane hydrate content; (4) the strength of ice specimens are higher than that of methane hydrate-ice mixture specimens; Based on the experimental data, the relationship among failure strength, confining pressure and methane hydrate content was obtained, and a modified Mohr-Coulomb criterion considering the influence of methane hydrate content on shear strength was proposed.

Keywords: methane hydrate; mechanical properties; safe extraction

Nomenclature

c = cohesion (MPa)

R^2 = coefficient of determination

T = temperature (°C)

ε = strain rate (%/min)

σ = normal stress at failure plane (MPa)

σ_1 = major principal stress at failure (MPa)

σ_2 = secondary principal stress (MPa)

σ_3 = minor principal stress or confining pressure (MPa)

$(\sigma_1 - \sigma_3)_{\max}$ = maximum deviator stress or failure strength (MPa)

τ = shear stress at failure (MPa)

φ = internal friction angle (°)

ω_h = methane hydrate content

1. Introduction

Methane hydrate is a solid clathrate compound in which a large amount of methane is trapped within a water crystal structure, forming a solid similar to ice [1–3]. It generally exists in sediment below the seafloor on continental margins and permafrost regions where there are suitable conditions of low temperature and high pressure [4–7]. The total amounts of methane trapped in methane hydrates is conservatively estimated to total twice the amount of carbon stored in all known fossil fuels on Earth [8,9]. However, safely extracting gas from methane hydrates faces still many potentially insurmountable technical issues that must be resolved. In view of the problems experienced during mining and drilling, the mechanical properties of methane hydrate are important to ensure sustainable production [10].

Deformation behavior and failure strength of methane hydrate during methane hydrate extraction are not clearly understood. The acoustic properties of methane hydrate have been studied to some extent [11,12], and studies on failure strength of methane hydrate-bearing sediments can be found in the literature [13–16]. Hyodo *et al.* [13] studied the failure strength of methane hydrate-bearing sediments with various degrees of hydrate saturation. Winters *et al.* [12] studied the dependence of shear strength of gas hydrate-bearing sediment on pore space contents, and the acoustic properties of gas hydrates and ice. Durham *et al.* [17] studied the strength and rheology of methane clathrate hydrates. In previous work, we preliminary studied the effect of temperature, confining pressure, strain rate and porosity on the mechanical properties of laboratory-formed methane hydrate and methane hydrate-bearing sediments [18–22]. A constitutive model describing the stress-strain behavior for methane hydrate-bearing sediment was established [20,21]. However, the mechanical properties of methane hydrate-ice mixture were rarely investigated. The natural methane hydrates are commonly observed occurring as disseminated grains, massive layers of pure hydrate, nodules that grow and displace surrounding sediments and veins filling small fractures [23,24]. Examples of heterogeneous distribution with zones of sparse or no hydrate interspersed with zones of high concentration are commonly found [25,26]. During the Deep Sea Drilling Project (DSDP) Leg 84 a core 1 m long and 6 cm in diameter of massive gas hydrate was recovered at Site 570 in upper slope sediment of the

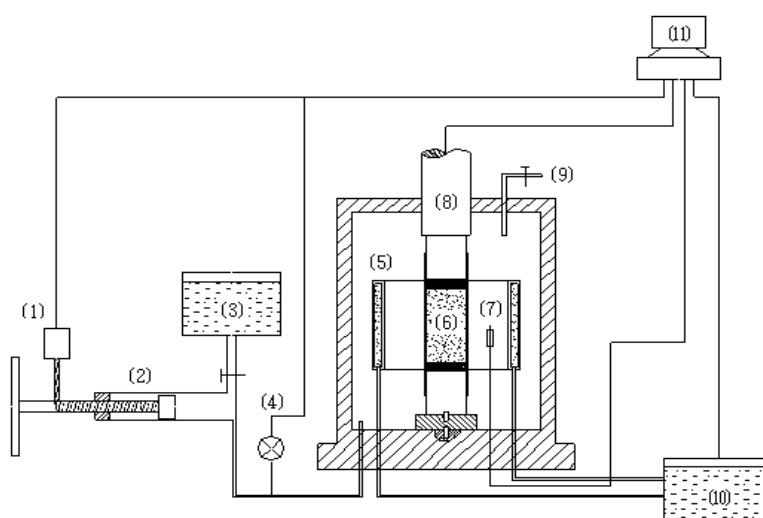
Middle America Trench offshore of Guatemala. This core contained only 5–7% sediment, the remainder being a solid hydrate composed of gas and water [27]. Methane hydrate formed in deposits under permafrost conditions is always mixed with ice. For massive layers of methane hydrate and heterogeneous samples, it is required to study the properties of both methane hydrates and sediments. Characterization the mechanical properties of methane hydrate-ice mixture are important to safely extract methane from methane hydrate reservoirs in permafrost regions.

In this study, a series of triaxial compression tests were conducted on laboratory-formed methane hydrate-ice mixtures with various methane hydrate contents under various confining pressures. Axial loading was conducted at an axial strain rate of 1.33%/min and a constant temperature of $-10\text{ }^{\circ}\text{C}$. The effects of confining pressure and methane hydrate content on the mechanical properties of methane hydrate-ice mixture were clarified.

2. Experimental Apparatus and Test Conditions

All the tests were conducted by using a TAW-60 triaxial testing device at low-temperature and high-pressure. The schematic diagram of the TAW-60 is shown in Figure 1 [17]. It can simulate *in situ* pressure and temperature conditions in a cylindrical sample which is typically 50 mm in diameter by 75–100 mm high. A test specimen is jacketed in the pressure chamber of the TAW-60 using a rubber membrane of 0.5 mm in thickness. A hydraulic servopump is used to maintain the confining pressure surrounding the specimen. A bath circulator is used to control the temperature of specimens by circulating liquid and a heat exchanger is located in the pressure chamber. A thermocouple (with accuracy of $0.5\text{ }^{\circ}\text{C}$) and a pressure sensor (with accuracy of 0.01 MPa) are placed in the pressure chamber to measure temperature and confining pressure.

Figure 1. The schematic diagram of TAW-60 triaxial testing device. (1) Stepping motor; (2) Pump; (3) Hydraulic oil tank; (4) Pressure gauge; (5) Heat exchanger; (6) Specimen; (7) Thermocouple; (8) Load cell; (9) Air pressure line; (10) Thermostatic bath; (11) Computer.



In this study, methane hydrate was formed by mixing ice powder of $250\text{ }\mu\text{m}$ size and methane gas in a high-pressure reaction chamber (Figure 2). Firstly, ice was formed by freezing distilled water in a

refrigerator with a temperature of $-5\text{ }^{\circ}\text{C}$. Ice powder was manufactured by using an ice crusher and sieved on a 60 mesh screen under a temperature of $-10\text{ }^{\circ}\text{C}$. Next, ice powder was put into the high-pressure reaction chamber, which was placed in a refrigerator and kept at a temperature of $-5\text{ }^{\circ}\text{C}$. Thirdly, high pressure methane gas of 10 MPa was injected into the chamber through a connecting hose and kept for 24 h. That the ice and methane gas had been fully reacted was indicated when no obvious pressure drop was observed. The content of methane hydrate was calculated by the difference between the mass of methane hydrate-ice mixture sample before and after dissociation. In this way, the obtained content or volume fraction of methane hydrate was about 30%. The synthetic methane hydrate-ice mixture was well-mixed with a predetermined amount of ice powder by stirring under a temperature of $-10\text{ }^{\circ}\text{C}$, and then methane hydrate-ice mixtures with various content of methane hydrate were obtained. The well-mixed methane hydrate-ice mixtures were put into a pressure molding device, and then cylindrical specimens (50 mm diameter \times 75 mm height) were formed under a controlled temperature ($-10\text{ }^{\circ}\text{C}$) and axial pressure (10 MPa). The prepared specimen was placed on the pedestal of the TAW-60, wrapped with a rubber membrane. When the hydraulic oil and specimen reached the designated temperature, the confining pressure and loading were applied. The tests were conducted on hydrate-ice mixture specimens under undrained conditions. The pore pressures remained constant during the axial loading. In order to reduce dissociation of methane hydrate or thawing of ice, all the test processes, including samples preparation were completed as soon as possible under cold storage ($-10\text{ }^{\circ}\text{C}$), and the hydraulic oil was cooled down before the installation of specimen into pressure chamber. A series of laboratory tests on formed methane hydrate-ice mixtures with various methane hydrate content were carried out under a confining pressure of 2.5 MPa, 5 MPa, 10 MPa, a temperature of $-10\text{ }^{\circ}\text{C}$ and a strain rate of 1.33%/min, as shown in Table 1. The density of specimens is 0.9 g/cm^3 , the porosity of specimens is 17.8%.

Figure 2. The schematic diagram of high-pressure reaction chamber.

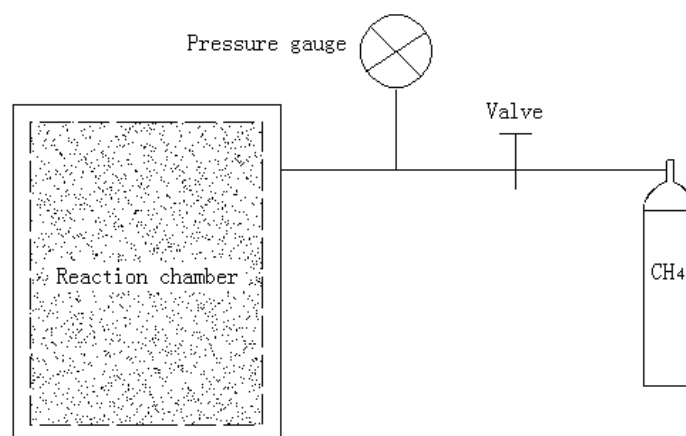


Table 1. Experimental condition of triaxial compression tests on methane hydrate-ice mixture.

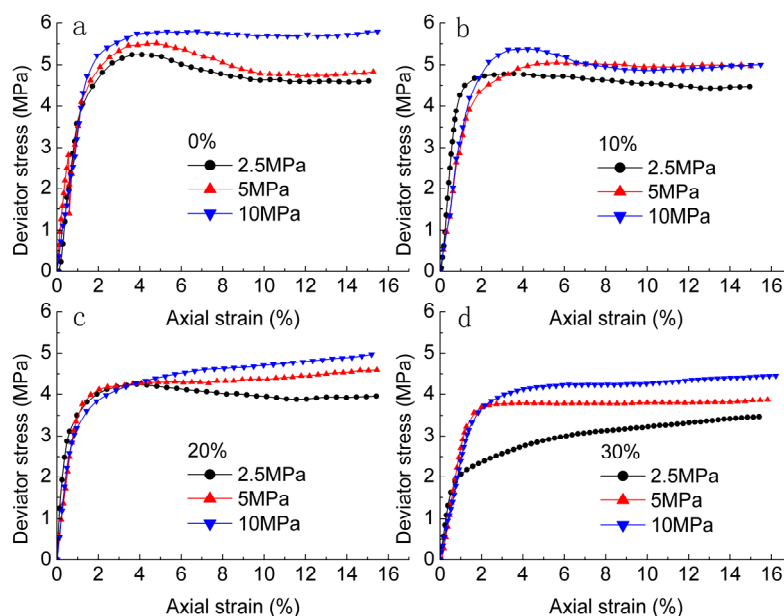
Temperature T	Strain rate ε	Methane hydrate content ω_h	Confining pressure (MPa) σ_3
$-10\text{ }^{\circ}\text{C}$	1.33%/min	0%	2.5, 5, 10
		10%	2.5, 5, 10
		20%	2.5, 5, 10
		30%	2.5, 5, 10

3. Results and Discussion

3.1. Stress-Strain Curves of Methane Hydrate-Ice Mixture

The stress-strain curves obtained from triaxial compression tests of methane hydrate-ice mixture with various methane hydrate content are shown in Figure 3. The deviator stress is defined as the stress after subtracting confining pressure from axial stress. The axial strain is calculated by the axial displacement divided by the initial height of specimen. From Figure 3, it can be observed that the deviator stress increases linearly with increasing axial strain when the axial strain is less than 1%. With further increases of axial strain, the slopes of stress-strain curves decrease gradually. Strain softening behavior is apparent for specimens with methane hydrate contents of 0% and 10% under all confining pressures, and specimen with methane hydrate content of 20% at a confining pressure of 2.5 MPa. Strain hardening behavior is presented for specimens with methane hydrate content of 20% at confining pressures of 5 MPa and 10 MPa, and specimens with methane hydrate content of 30%, thus indicates that the deformation characteristic is strongly affected by the confining pressure and methane hydrate content. Strain hardening became more apparent with increasing confining pressure and methane hydrate content. It is considered that crack propagation in methane hydrate-ice mixtures is associated with the formation of microcracks at the crack tip, and interlocking of particles behind the crack tip. The increasing confining pressure may restrict the growth of microcracks and the deformation of specimens, which leads to increases in interparticle coordination and frictional resistance. Hydrate particles altered the cohesion and enhanced the bite force between hydrates and ices. In the beginning of the crack growth, the stress-strain curves consist of some linear parts but near the fracture toughness they become non-linear. The slope of the stress-strain curves increases with the higher confining pressure [28] and methane hydrate content.

Figure 3. Stress-strain curves of methane hydrate-ice mixture with methane hydrate content of (a) 0%, (b) 10%, (c) 20% and (d) 30%.



3.2. Effects of Confining Pressure and Methane Hydrate Content on Failure Strength

In this study, the peak value of deviator stress during the compression under axial strain reaching 15% is taken as failure strength. Figure 4 shows the failure strength plotted against the confining pressure. It indicates that the failure strengths are significantly increased with confining pressure when confining pressures are less than 10 MPa. This occurs because the increasing confining pressure restricts the growth of fractures, which may increase the interparticle coordination and frictional resistance, and consequently increases the strength of samples. There is a little difference with our previous work on methane hydrate-bearing sediments [17]. When the confining pressure is more than 5 MPa, the strength of methane hydrate-bearing sediments starts decreasing slowly with the increase of confining pressure. It is considered that the sand particles cause the decrease of strength. Some particles are crushed, and the pore-ice melting at grain-to-grain because of the stress concentration, which lead the decline of strength. According to the literatures [29,30], the effect of the interphase on the stress concentration strongly depends on the ratio between the elastic modulus of the matrix and the interphase and on the Poisson's ratio of the interphase. The consideration of an interphase leads to a non-uniform stress distribution within the particle. The physical/chemical properties of ice are similar to that of hydrates, but dramatically different to that of sand particles. Stress concentration is smaller between ice and hydrate than between ice and sand particle. It also can be observed that the failure strengths of methane hydrate-ice mixture specimens strongly depend on methane hydrate content.

Figure 4. Effect of confining pressure on failure strength of methane hydrate-ice mixture, and a comparison of calculated results and experimental results.

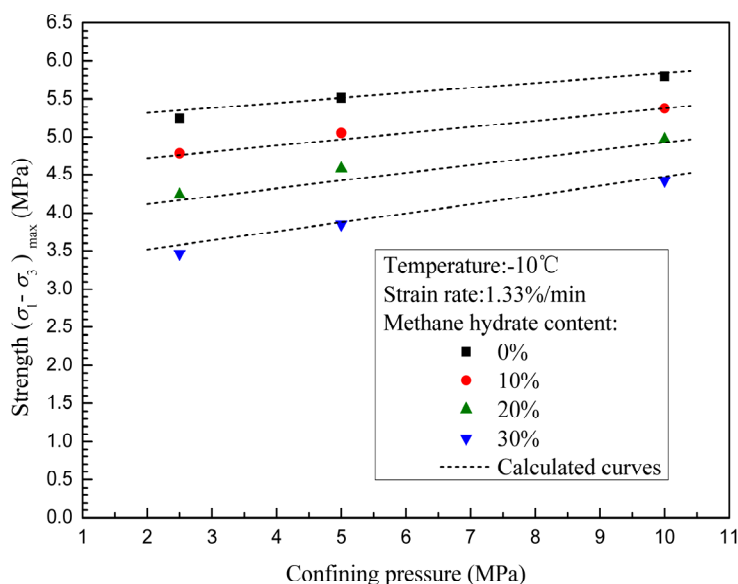
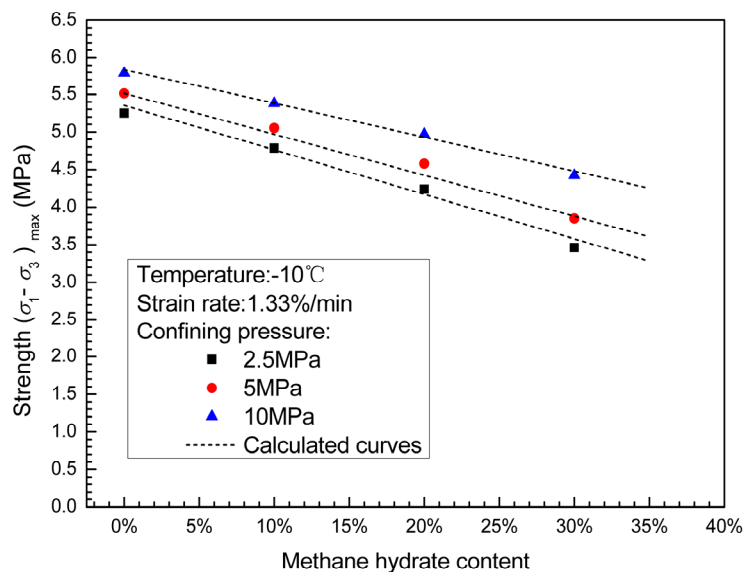


Figure 5 shows the strength and the dependency as a function of methane hydrate content under various confining pressures of 2.5 MPa, 5 MPa, and 10 MPa. The failure strength varies with methane hydrate content—the larger the methane hydrate content, the smaller the failure strength. Methane hydrate changes the cementing status between ice particles, and the cohesion between ice particles is larger than that between ice and methane hydrate particles. In the case of specimens with methane

hydrate content of 0%, the failure strength rises from 5.25 MPa to 5.792 MPa as the confining pressure increases from 2.5 MPa to 10 MPa. The increment of failure strength is 0.512 MPa. In the case of specimen with methane hydrate contents of 10%, 20% and 30%, the increments of failure strength are 0.597 MPa, 0.73 MPa, and 0.961 MPa, respectively, indicating that confining pressure increasingly impacts failure strength of methane hydrate-ice mixture specimen with increasing methane hydrate content. It also means that the internal friction angle increases with increase of methane hydrate content; the friction force between ice particles is smaller than that between ice and methane hydrate particles.

Figure 5. Effect of methane hydrate content on failure strength of methane hydrate-ice mixture, and a comparison of calculated results and experimental results.



The increments of failure strength are 1.788 MPa, 1.664 MPa and 1.369 MPa as the methane hydrate content increases from 0% to 30% under confining pressures of 2.5 MPa, 5 MPa and 10 MPa, respectively. The failure strength shows a more obvious dependence on methane hydrate content at higher confining pressures. This may be caused by the pressure sensitivity of methane hydrate. Confining pressure may suppress the dissociation of methane hydrate.

3.3. Failure Strength and Shear Strength

The purpose of strength criteria is to predict or estimate the failure of materials, and to guide engineering design. In this study, the Mohr-Coulomb criterion is used to describe the failure behavior of methane hydrate-ice mixture specimens. According to the Mohr-Coulomb criterion, cohesion and internal friction angle are two key factors to evaluate the shear strength of materials. Cohesion reflects the synthesis action of physical-chemical forces between particles, such as Van der Waals forces and cementing forces. The internal friction angle represents the friction characteristic of materials, including surface friction force and interlocking force of particles.

For a conventional triaxial test, $\sigma_1 > \sigma_2 = \sigma_3$, the Mohr-Coulomb criterion can be described by following equation:

$$\sigma_1 = A\sigma_3 + B \quad (1)$$

where, $A = \frac{1 + \sin \phi}{1 - \sin \phi}$, $B = \frac{2c \cos \phi}{1 - \sin \phi}$, σ_1 is the major principal stress at failure, σ_3 is the confining pressure or minor principal stress, c is the cohesion, ϕ is the internal friction angle. The values of c and ϕ can be obtained by the Mohr-Coulomb criterion, as shown in Figures 6(a–d). Table 2 shows the experimental parameters A and B , the cohesion c and internal friction angle ϕ of methane hydrate-ice mixture specimen with various methane hydrate content tested at a temperature of -10°C .

Figure 6. The strength envelopes and Mohr circles of methane hydrate-ice mixtures with various methane hydrate content of (a) 0%, (b) 10%, (c) 20% and (d) 30%.

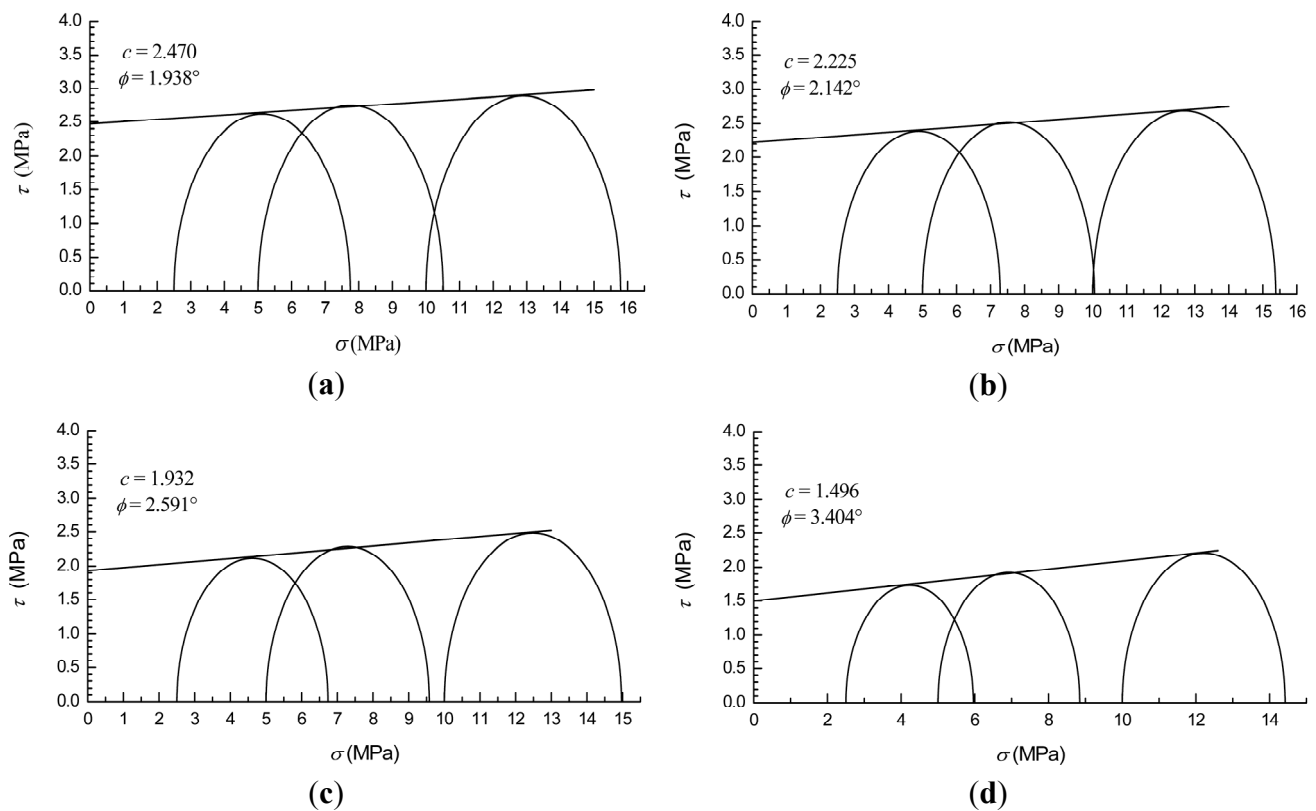


Table 2. Experimental parameters obtained by Mohr-Coulomb criterion.

Methane Hydrate Content ω_h	A	B (MPa)	c (MPa)	ϕ ($^\circ$)
0%	1.070	5.110	2.47	1.938
10%	1.078	4.620	2.225	2.142
20%	1.095	4.043	1.932	2.591
30%	1.126	3.175	1.496	3.404

From Table 2, it can be clearly observed that the cohesion decreases with increasing methane hydrate content, while the internal friction angle increases with increasing methane hydrate content. However, the effect of methane hydrate content on internal friction angle is not significant. The internal friction angle rises from 1.938° to 3.404° as the methane hydrate content increases from 0% to 30%, the increment of internal friction angle is only 1.5° .

Based on the experimental data in Table 2, the relationships between A , B and methane hydrate content are obtained, and can be described respectively as follows:

$$A = 1.0642 + 0.1857\omega_h \quad (2)$$

$$B = 5.194 - 6.38\omega_h \quad (3)$$

Here, ω_h is methane hydrate content, $R_A^2 = 0.8843$, $R_B^2 = 0.9727$.

From Equation (1), we have:

$$(\sigma_1 - \sigma_3)_{\max} = (A-1)\sigma_3 + B \quad (4)$$

Substituting Equations (2), (3) into Equation (4), we can obtain the relationship between failure strength and confining pressure σ_3 , methane hydrate content ω_h . Namely:

$$(\sigma_1 - \sigma_3)_{\max} = 5.194 - 6.38\omega_h + 0.0642\sigma_3 + 0.1857\omega_h\sigma_3 \quad (5)$$

Based on Equation (5), a comparison is made between the experimental values and calculated values, and the results are shown in Figures 4 and 5. The proposed equation can be taken to predict the failure strength of methane hydrate-ice mixture with various methane hydrate content under certain conditions.

Shear stress of a material is the internal resistance per unit area that the material can offer to resist failure and sliding along any plane inside it. As stated by the Mohr-Coulomb failure criterion, failure by shear will occur when the shear on a failure plane reaches a certain value. And this value can be deduced by the strength envelope of materials. The strength envelope can be expressed as:

$$\tau = c + \sigma \tan \phi \quad (6)$$

where τ is the shear stress at failure, σ is the normal stress at the failure plane. From Table 2, the relationship between cohesion c , ϕ and methane hydrate content ω_h can be described respectively as follows:

$$c = 2.513 - 3.215\omega_h \quad (7)$$

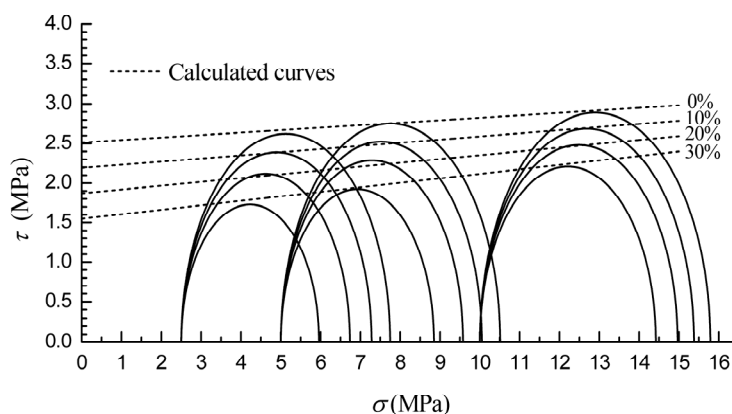
$$\tan \phi = 0.0313 + 0.0848\omega_h \quad (8)$$

Here, $R_c^2 = 0.9818$, $R_{\tan \phi}^2 = 0.9262$.

Substituting Equations (7), (8) into Equation (6), the expression of strength envelope becomes this:

$$\tau = 2.513 - 3.215\omega_h + 0.0313\sigma + 0.0848\omega_h\sigma \quad (9)$$

Figure 7 shows the Mohr circles and the calculated strength envelopes of methane hydrate-ice mixture specimens with various methane hydrate content of 0%, 10%, 20% and 30% at a temperature of -10 °C. It can be seen that the Mohr-Coulomb criterion is still acceptable for methane hydrate-ice mixtures with various methane hydrate contents under a confining pressure of less than 10 MPa. While drilling for exploration and exploitation of gas hydrate reservoir in permafrost region, it can be used for the purposes of engineering design and optimization.

Figure 7. Comparisons between experimental results and calculated results.

4. Conclusions

To acquire more knowledge about the mechanical properties of methane hydrate, a series of triaxial compression tests were carried out on laboratory-formed methane hydrate-ice mixtures with various methane hydrate contents of 0%, 10%, 20% and 30%. Axial loading was conducted at an axial strain rate of 1.33%/min and a constant temperature of $-10\text{ }^{\circ}\text{C}$. The failure strength and the behavior of stress-strain curves of methane hydrate-ice mixtures were analyzed. The following conclusions are drawn based on this study:

- (1) The deformation characteristic is strongly affected by confining pressure and methane hydrate content. Strain hardening in the stress-strain relationship became stronger with increase in confining pressure and methane hydrate content.
- (2) The failure strengths of methane hydrate-ice mixture specimens are significantly increased with confining pressure when confining pressure is less than 10 MPa. Confining pressure increasingly impacts on failure strength with increasing methane hydrate content, which means that the internal friction angle increases with methane hydrate content.
- (3) The failure strengths of methane hydrate-ice mixture specimens decreases with methane hydrate content, and shows a more significant dependence on methane hydrate content at higher confining pressure.
- (4) The cohesion of methane hydrate-ice mixture specimens decreases with methane hydrate content, and the strength of ice specimens are higher than that of methane hydrate-ice mixture specimens.

Based on the experimental data, the relationships among failure strength, confining pressure and methane hydrate content was obtained, and a modified Mohr-Coulomb criterion considering the influence of methane hydrate content on failure strength was proposed. They agree well with the experimental data, and can be taken to predict failure strength of methane hydrate-ice mixtures with various methane hydrate content under a confining pressure less than 10 MPa, a temperature of $-10\text{ }^{\circ}\text{C}$. Further investigations on the mechanical properties of methane hydrate under various temperatures and strain rates are recommended.

Acknowledgments

This work was supported by a grant from the Major National S&T Program (No. 2011ZX05026-004), the Major State Basic Research Development Program of China (973 Program) (No. 2009CB219507).

References

1. Ripmeester, J.A.; Ratcliffe, C.I. Low-temperature cross-polarization/magic angle spinning ^{13}C NMR of solid methane hydrates: Structure, cage occupancy, and hydration number. *J. Phys. Chem.* **1988**, *92*, 337–339.
2. Ripmeester, J.A.; Tse, J.S.; Ratcliffe, C.I.; Powell, B.M. A new clathrate hydrate structure. *Nature* **1987**, *325*, 135–136.
3. Sloan, E.D. Gas hydrates: Review of physical/chemical properties. *Energy Fuels* **1998**, *12*, 191–196.
4. Suess, E.; Bohrmann, G.; Greinert, J.; Lausch, E. Flammable ice. *Sci. Am.* **1999**, *281*, 76–83.
5. MacDonald, I.R.; Guinasso, N.L.; Sassen, R.; Brooks, J.M.; Lee, L.; Scott, K.T. Gas hydrate that breaches the sea floor on the continental slope of the Gulf of Mexico. *Geology* **1994**, *22*, 699–702.
6. Hoffmann, R. Old gas, new gas. *Am. Sci.* **2006**, *94*, 16–18.
7. Kvenvolden, K.A.; Ginsburg, G.D.; Soloviev, V.A. Worldwide distribution of subaquatic gas hydrates. *Geo-Mar. Lett.* **1993**, *13*, 32–40.
8. Kvenvolden, K.A. Methane hydrate—A major reservoir of carbon in the shallow geosphere? *Chem. Geol.* **1988**, *71*, 41–51.
9. Collett, T.S. Energy resource potential of natural gas hydrates. *AAPG Bull.* **2002**, *86*, 1971–1992.
10. Goodman, A. *In situ* Gas Hydrates: Past Experience and Exploitation Concepts. In *Proceedings of the International Gas Research Conference*, Chicago, IL, USA, 9–12 June 1980; pp. 376–391.
11. Winters, W.J.; Pecher, I.A.; Waite, W.F.; Mason, D.H. Physical properties and rock physics models of sediment containing natural and laboratory-formed methane gas hydrate. *Am. Miner.* **2004**, *89*, 1221–1227.
12. Winters, W.J.; Waite, W.F.; Mason, D.H.; Gilbert, L.Y.; Pecher, I.A. Methane gas hydrate effect on sediment acoustic and strength properties. *J. Petrol. Sci. Eng.* **2007**, *56*, 127–135.
13. Hyodo, M.; Nakata, Y.; Yoshimoto, N.; Ebinuma, T. Basic research on the mechanical behavior of methane hydrate-sediments mixture. *Soils Found.* **2005**, *45*, 75–85.
14. Miyazaki, K.; Masui, A.; Tenma, N.; Ogata, Y.; Aoki, K. Study on mechanical behavior for methane hydrate sediment based on constant strain-rate test and unloading-reloading test under triaxial compression. *Int. J. Offshore Polar Eng.* **2010**, *20*, 61–67.
15. Miyazaki, K.; Masui, A.; Sakamoto, Y.; Aoki, K.; Tenma, N.; Ogata, Y.; Yamaguchi, T. Triaxial compressive properties of artificial methane-hydrate-bearing sediment. *J. Geophys. Res.* **2011**, *116*, doi:10.1029/2010JB008049.
16. Miyazaki, K.; Tenma, N.; Aoki, K. Effects of confining pressure on mechanical properties of artificial methane-hydrate-bearing sediment in triaxial compression test. *Int. J. Offshore Polar Eng.* **2011**, *21*, 148–154.

17. Durham, W.B.; Kirby, S.H.; Stern, L.A.; Zhang, W. The strength and rheology of methane clathrate hydrate. *J. Geophys. Res.* **2003**, *108*, doi:10.1029/2002JB001872.
18. Li, Y.H.; Song, Y.C.; Yu, F.; Liu, W.G.; Zhao, J.F. Experimental study on mechanical properties of gas hydrate-bearing sediments using kaolin clay. *China Ocean Eng.* **2011**, *25*, 113–122.
19. Song, Y.C.; Yu, F.; Li, Y.H.; Liu, W.G.; Zhao, J.F. Mechanical property of artificial methane hydrate under triaxial compression. *J. Nat. Gas Chem.* **2010**, *19*, 246–250.
20. Yu, F.; Song, Y.C.; Li, Y.H.; Liu, W.G.; Lam, W.H. Analysis of stress-strain behavior and constitutive relation of methane hydrate-bearing sediments with various porosity. *Int. J. Offshore Polar Eng.* **2011**, *21*, 316–322.
21. Yu, F.; Song, Y.C.; Liu, W.G.; Li, Y.H.; Lam, W.H. Analyses of stress strain behavior and constitutive model of artificial methane hydrate. *J. Petrol. Sci. Eng.* **2011**, *77*, 183–188.
22. Li, Y.H.; Song, Y.C.; Yu, F.; Liu, W.G.; Wang, R. Effect of confining pressure on mechanical behavior of methane hydrate-bearing sediments. *Petrol. Explor. Dev.* **2011**, *38*, 637–640.
23. Haeckel, M.; Suess, E.; Wallmann, K.; Rickert, D. Rising methane gas bubbles form massive hydrate layers at the seafloor. *Geochim. Cosmochim. Acta* **2004**, *68*, 4335–4345.
24. Yuan, T.; Nahar, K.S.; Chand, R.; Hyndman, R.D.; Spence, G.D.; Chapman, N.R. Marine gas hydrates: Seismic observations of bottom-simulating reflectors off the West Coast of Canada and the East Coast of India. *Geohorizons* **1998**, *3*, 1–11.
25. Bohrmann, G.; Kuhs, W.F.; Klapp, S.A.; Techmer, K.S.; Klein, H.; Murshed, M.; Abegg, F. Appearance and preservation of natural gas hydrate from Hydrate Ridge sampled during ODP Leg 204 drilling. *Mar. Geol.* **2007**, *244*, 1–14.
26. Kleinberg, R.L.; Flaum, C.; Straley, C.; Brewer, P.G.; Malby, G.E.; Peltzer, E.T.; Friederich, G.; Yesinowski, J.P. Seafloor nuclear magnetic resonance assay of methane hydrate in sediment and rock. *J. Geophys. Res.* **2003**, *108*, doi:10.1029/2001JB000919.
27. Kvenvolden, K.A.; Claypool, G.E.; Threlkeld, C.N.; Sloan, E.D. Geochemistry of a naturally occurring massive marine gas hydrate. *Org. Geochem.* **1984**, *6*, 703–713.
28. Vásárhelyi, B. Investigation of Crack Propagation with Different Confining Pressure on anisotropic Gneiss. In *Rock Mechanics—A Challenge for Society*; Särkkä, P., Eloranta, P., Eds.; Taylor & Francis: Lisse, The Netherlands, 2001; pp. 187–190.
29. Lauke, B.; Schüller, T. Calculation of stress concentration caused by a coated particle in polymer matrix to determine adhesion strength at the interface. *Compos. Sci. Technol.* **2002**, *62*, 1965–1978.
30. Huang, M.S.; Li, Z.H. Influences of particle size and interface energy on the stress concentration induced by the oblate spheroidal particle and the void nucleation mechanism. *Int. J. Solids Struct.* **2006**, *43*, 4097–4115.